minerals

MDPI

Article

Genetic Mechanisms and Main Controlling Factors of Dolomite Reservoirs in Member 1 of the Lower Cambrian Canglangpu Formation, Northern–Central Sichuan Basin

Fei Huo [1,2,3,4], Chuan He [1,2], Xueyan Wu [3,4,*], Zhengdong Wang [3,4], Kezhong Li [3,4], Zhidian Xi [3,4], Yi Hu [3,4], Zhun Wang [3,4] and Binxiu Li [3,4]

1 State Key Laboratory of Shale Oil and Gas Enrichment Mechanisms and Effective Development, Beijing 100083, China; huofei342099206@163.com (F.H.)
2 SINOPEC Key Laboratory of Petroleum Accumulation Mechanisms, Wuxi 214126, China
3 State Key Laboratory of Oil and Gas Reservoir Geology and Exploitation, Southwest Petroleum University, Chengdu 610500, China
4 School of Geoscience and Technology, Southwest Petroleum University, Chengdu 610500, China
* Correspondence: 202421000060@stu.swpu.edu.cn

Abstract

In recent years, oil and gas exploration in the Lower Cambrian of the central–northern Sichuan Basin, China, has demonstrated enormous resource potential. As a potential interval of high-quality hydrocarbon source rocks, the Canglangpu Formation of the Lower Cambrian remains underdeveloped in exploration and lacks in-depth research. Affected by tectonics, sedimentary environment, and diagenesis, the genetic mechanisms and genetic models of carbonate reservoirs in the Canglangpu Formation within the study area need further clarification. This study utilizes petrological characteristics of dolomite and geochemical data to clarify diagenetic fluids of different reservoir rocks and identifies the main controlling factors and development models of the reservoirs. The results show that the dolomites in Member 1 of the Canglangpu Formation (Cang-1 Member) in central–northern Sichuan are mainly classified into three types: silty–fine crystalline dolomite (D1), granular dolomite (D2), and residual-texture dolomite (D3). The reservoir spaces are dominated by intercrystalline pores, intergranular pores, and structural fractures. The porosity of the Cang-1 Member in the area is relatively low, with an average porosity of 5% or lower. The reservoir porosity average is 3.63%, belonging to low-porosity reservoirs. The permeability average is 2.94×10^{-3} mD. Analysis of different geochemical indicators indicates that the diagenetic fluids of the three dolomite types are mainly syndepositional seawater. D1 is formed by penecontemporaneous dolomitization, while both D2 and D3 are formed during the shallow-to-middle burial stage. The main controlling factors of dolomite reservoirs include sedimentary facies, diagenesis, and tectonic movement. This study clarifies the genesis and development model of dolomite reservoirs in the Cang-1 Member, aiming to provide reliable and valuable references for the exploration of dolomite reservoirs in the Canglangpu Formation of the Sichuan Basin.

Keywords: central–northern Sichuan basin; Canglangpu formation; origin of dolomite; main controlling factors of reservoirs; evolutionary model

Check for updates

Academic Editor: Georgia Pe-Piper

Received: 21 November 2025
Revised: 16 January 2026
Accepted: 17 January 2026
Published: 28 February 2026

Copyright: © 2026 by the authors. Licensee MDPI, Basel, Switzerland. This article is an open access article distributed under the terms and conditions of the Creative Commons Attribution (CC BY) license.

1. Introduction

With the advancement of oil and gas exploration and research, deep and ultra-deep oil and gas fields have become key targets of global oil and gas exploration [1]. According

to data analysis of large global petroliferous basins, dolomite can serve as a high-quality reservoir rock for carbonates under deep burial conditions [1,2], and the degree and process of dolomitization are closely related to the exploration and development of high-quality reservoirs [3–5]. Over the past few decades, the occurrence, evolutionary models, and genetic mechanisms of dolomite have been hot topics in global carbonate rock research [6–10]. A variety of different models have been proposed, mainly including the mixed-water dolomitization model, reflux seepage dolomitization model, burial dolomitization model, hydrothermal dolomitization model, and thermal convection model [11–15]. However, the development laws and formation mechanisms of dolomite reservoirs have not been clearly defined. Therefore, it is crucial to understand the source of diagenetic fluids for dolomite and the genetic models of reservoirs.

As an important natural gas exploration and development base in China, the Sichuan Basin has demonstrated enormous resource potential in the Sinian System and the Lower Paleozoic Cambrian System in recent years. The accumulated declared three-level geological reserves have exceeded one trillion cubic meters, yet the overall resource discovery rate is merely 17.5% [16–19], leaving substantial room for further exploration. For a long time, the focus of exploration and research has been concentrated on well-known high-quality reservoirs such as the Longwangmiao Formation and the Dengying Formation [20–22]. In contrast, the Cambrian Canglangpu Formation, as a potential reservoir interval adjacent to the high-quality source rocks of the Qiongzhusi Formation, has not received sufficient attention due to factors including great burial depth, low research intensity, and complex reservoir characteristics [23,24]. Drilled in eastern Sichuan in January 2018, wildcat well Wutan-1 confirmed the Dazhou–Kaijiang paleohigh and reservoirs in the Longwangmiao and Dengying Formations and first encountered 50 m thick Canglangpu dolomites in local ultra-deep wells. Re-examination of old wells and outcrops revealed extensive Canglangpu dolomites with potential reservoirs, while Gaoshiti–Moxi wells showed favorable logging responses. On 16 October 2020, Well Jiaotan-1 yielded 516,200 m^3/d of industrial gas, achieving the first Canglangpu exploration breakthrough; this formation, adjacent to Qiongzhusi source rocks, has unique accumulation advantages and is a key wildcat target. Specifically, although some studies have been conducted on the genetic mechanism of dolomite in the Canglangpu Formation [25,26], relevant research on the dolomite reservoirs of this formation in the central and northern Sichuan Basin remains quite limited. Controlled by the combined effects of paleotectonics, sedimentary environment, diagenesis, and other factors, the genetic mechanism of these reservoirs is intricate. Additionally, the genetic models and distribution rules of the reservoirs remain unclear, and relevant in-depth research is still lacking.

In light of the limited systematic understanding of the genetic models and main controlling factors of dolomite reservoirs in the Canglangpu Formation of the north–central Sichuan Basin, as previous studies have primarily focused on other key intervals, this study integrates field profile measurements, drilling core observations, and geochemical data from the Canglangpu Formation in the Sichuan Basin. It systematically analyzes the petrological characteristics of dolomite reservoirs, investigates the genetic mechanisms of dolomitization, and clarifies the main controlling factors and evolutionary models of reservoir development, thereby addressing the research gap in this field. The findings aim to provide a theoretical basis and practical guidance for oil and gas exploration in the Canglangpu Formation of the Sichuan Basin while also offering valuable insights for further research on dolomite-related scientific issues.

2. Geological Setting

The Sichuan Basin is located in southwestern China and has experienced the superposition of multiple tectonic movements, resulting in a complex current tectonic framework within the basin. It can be divided into five secondary tectonic units, namely the Eastern Sichuan Paleo-slope Central Uplift High-steep Fault-fold Belt, Southern Sichuan Paleo-depression Central Uplift Low-steep Dome Belt, Central Sichuan Paleo-uplift Central Slope Gentle Belt, Western Sichuan Meso-Cenozoic Depression Low-steep Belt, and Northern Sichuan Paleo-Central Depression Low-gentle Belt [27–29]. The study area is situated in the central and northern Sichuan Basin (central–northern Sichuan region) (Figure 1a), with geographical coordinates ranging from 28° N to 32°40′ N latitude and 102°30′ E to 110° E longitude, covering a total area of approximately 17 × 10^4 km^2.

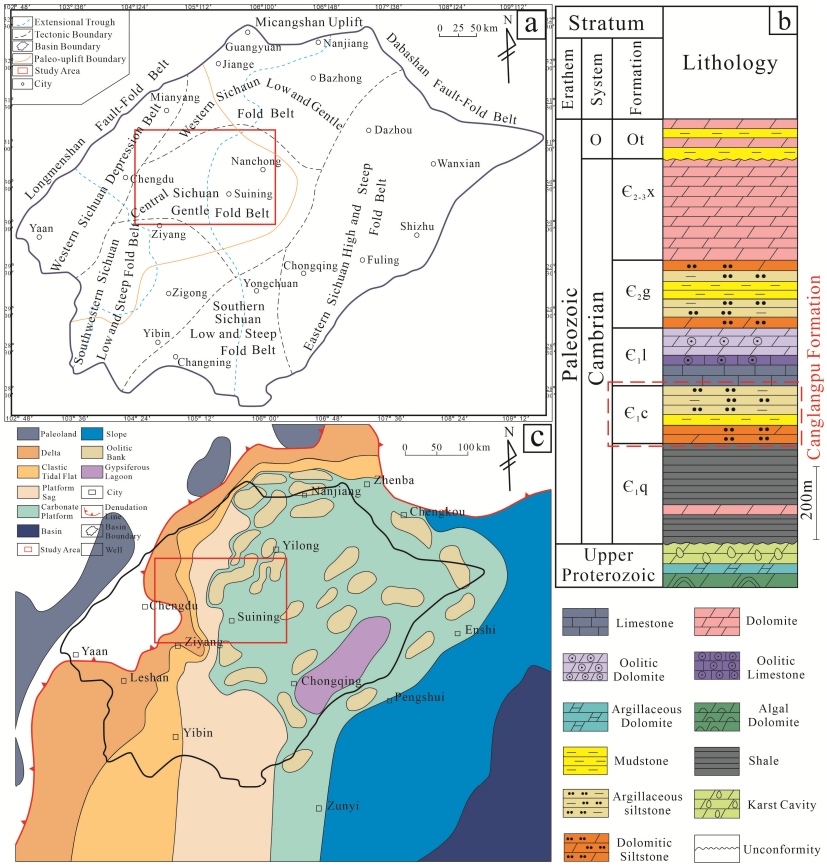

Figure 1. Simplified geological background map of the Sichuan Basin. (**a**) Map of geographical and tectonic location of the Sichuan Basin. (**b**) Generalized Cambrian lithostratigraphic column for eastern–northern Sichuan Basin [27]. (**c**) Palaeogeographic map of the Canglangpu Formation interval, Sichuan Basin, ("ϵ_1q, ϵ_1c, and ϵ_1l", respectively, represent the Lower Cambrian Qiongzhusi Formation, Canglangpu Formation, and Longwangmiao Formation).

The Cambrian strata in the Sichuan Basin are fully developed and mostly buried deep underground. The burial depth generally ranges from 2500 to 5000 m and can exceed 9000 m in the depression areas, with the stratum thickness varying between 0 and 1500 m [30–33]. Its lower boundary is in paraconformable contact with the Dengying Formation, while the upper boundary forms either paraconformable or conformable contact with the Ordovician System [34–36]. Among them, the Lower Cambrian can be further divided into three formations, namely, the Qiongzhusi Formation, Canglangpu Formation, and Longwangmiao Formation in ascending order (Figure 1b), and the Canglangpu Formation is subdivided from bottom to top into the first member (Cang-1 Member) and the

second member (Cang-2 Member) [37,38]. The Canglangpu Formation is dominated by a coastal-shelf sedimentary system [39–41]. During the sedimentary period of the Cang-1 Member, the sea level rose, and the paleogeomorphology was characterized by "high in the northwest and low in the southeast". The Kangdian Paleoland and Motianling Paleoland served as the provenance areas. The coastal facies was distributed in the northwestern margin, the shallow-water shelf facies constituted the main body, with grain banks developed in the high-lying parts of the paleouplift, and the deep-water shelf facies was confined to the rift troughs [42] (Figure 1c). During the sedimentary period of the Cang-2 Member, a large-scale regression occurred. The uplift of the Hannan Paleoland led to an increase in terrigenous clastic supply, resulting in the migration of sedimentary facies towards the interior of the basin. The scope of the coastal facies expanded; the shallow-water shelf facies remained the main body, but the proportion of clastic rocks increased, and the distribution range of the deep-water shelf facies narrowed [43,44]. Overall, the distribution of sedimentary facies is jointly controlled by paleogeomorphology, provenance, and sea level, following the rule of "paleolands controlling provenance and local uplifts controlling banks". The paleolands regulated the supply direction of terrigenous clastics, and the local high-lying areas were favorable for the accumulation of grains to form grain banks [45,46]. A sedimentary background that has laid a geological foundation for the subsequent classification of dolomite types, analysis of their formation mechanisms, and identification of the main controlling factors of reservoirs provide essential support for the research on dolomite reservoirs.

3. Materials and Methods

The samples used in this study and these experiments were mainly collected from the northern–central Sichuan region. Systematic sampling was conducted on intervals with well-developed dolomite in multiple wells including CT1 and GS10, and fresh samples were collected from outcrops with excellent exposure and extensive dolomite development in northern–central Sichuan; more than 100 samples were collected in total. This study mainly selected surface dolomite samples for comparison with deep-burial dolomite samples. All samples underwent systematic microscopic identification, and some samples were subjected to cathodoluminescence analysis. Meanwhile, samples intended for geochemical analysis were carefully sorted and selected under the microscope to avoid calcite veins and sparry calcite cements as much as possible, ensuring the reliability of the classified samples.

The X-ray diffraction (XRD) ordering degree analysis in this study was completed at the Petroleum Geology Experimental Center of Exploration and Development Research Institute, Zhongyuan Oilfield Company, Sinopec in Puyang, China. Dolomite identification was performed using the PDF-2 crystallographic database (PDF No. 75-1710 and 84-1208).

Carbon and oxygen isotope analysis was conducted at Yangtze University. The specific procedure is as follows: prior to testing, 10 mg of powder was micro-drilled under a binocular microscope, preprocessed by passing through a 200-mesh sieve. Approximately 200 μg of the sample was reacted with pure phosphoric acid at 70 °C, and the collected CO_2 was injected into a DELTA V Advantage SN09017D isotope ratio mass spectrometer (IRMS) by Thermo Fisher Scientific (Bremen, Germany) using He gas for analysis. The test was calibrated with a standard reference material (IAEA CO-8), and all test results were reported relative to the VPDB reference standard with a precision of ±0.1‰ [47].

Rare Earth Elements (REEs) analysis was carried out at the Key Laboratory of Carbonate Reservoirs, China National Petroleurm Corporation (CNPC, Beijing, China), Southwest Petroleum University (Chengdu, China). Prior to testing, samples were ultrasonicated for 90 min to remove surface impurities and then air-dried in a fume hood. The external standard for the test was the USGS MACS-3 carbonate powder pellet (U.S.Geological Survey),

the internal standard was Ca in stoichiometric dolomite, and the quality control standard was the carbonate ultra-fine pellet Jcp-1 [48].

Strontium isotope analysis was performed at the State Key Laboratory of Oil and Gas Reservoir Geology and Exploitation Engineering, Chengdu University of Technology. Prior to testing, samples were purified under a binocular microscope, followed by micro-drilling to collect 50 mg of powder. At room temperature, the powder was dissolved in 2 mL of 1 M ammonium acetate, ultrasonicated for 30 min, and centrifuged at 3000 rpm for 10 min. The insoluble fraction was leached with 3 mL of 2.5% acetic acid at 200 °C for 24 h. After drying, the sample was converted to chloride salt using 6 M hydrochloric acid (HCl), and strontium was separated via an ion exchange column prior to being introduced into a Thermo Fisher Scientific Triton Plus thermal ionization mass spectrometer (TIMS) manufactured by Thermo Fisher Scientific (Bremen, Germany) for analysis [49].

The cathodoluminescence (CL) experiment was conducted at the Chengdu Institute of Mineral Resources. Prior to testing, the samples were cleaned, and fresh surfaces were cut to prepare 300 thin sections. First, the petrological and mineralogical characteristics were observed under a standard polarizing microscope. Subsequently, experiments were conducted using cold cathodoluminescence technology with a CI8200 MK5-2 cathodoluminescence microscope manufactured by Cambridge Image Technology Ltd. (CITL) of Cambridge, UK, operating at an accelerating voltage of 12 kV and a beam current of 0.7 mA.

4. Results

4.1. Reservoir Rock Characteristics

Based on the results of thin section identification, *X*-ray diffraction (XRD), and scanning electron microscopy (SEM) analysis of the Cambrian Cang-1 Member in the study area, combined with the dolomite structural-genetic classification scheme [50], the dolomite reservoir rocks in the area are divided into three types according to their crystal size and surface morphology: silty–fine crystalline dolomite (D1), granular dolomite (D2), and residual granular textured dolomite (D3).

(1) Silty–Fine Crystalline Dolomite (D1)

D1 is widely developed in the study area. Under the microscope, it is mainly composed of hypidiomorphic–xenomorphic crystals with various grain structures and uneven sizes (Figure 2a), dominated by silty–fine crystalline dolomite (Figure 2b). Typically, this type of dolomite retains abundant protolith micrites or impurities, appearing as dirty brown under the microscope (Figure 2c). Obvious dolomite recrystallization can be observed (Figure 2d). Under cathodoluminescence, the silty–fine crystalline dolomite emits bright and uniform red light (Figure 2e), and some dolomite crystals exhibit the distinct "foggy core and bright rim" texture. Porosity is basically underdeveloped in this type of dolomite (Figure 2f).

(2) Granular Dolomite (D2)

The granular types in D2 are dominated by ooids (Figure 3a), bioclasts (Figure 3b), and a small amount of psammites. This type of dolomite is mainly characterized by replaced granular ghosts and granular textures, with dolomite content exceeding 90% in most cases and ooid content reaching over 70% in some samples. The grain size ranges from 0.5 to 2.0 mm. The cores and concentric laminae of ooids are composed of euhedral–hypidiomorphic silty–fine crystalline dolomite (Figure 3c). Intercrystalline pores and intergranular pores are well-developed, and asphalt filling can be observed in some pores (Figure 3d). Under cathodoluminescence, ooids emit weak dark red light, while the cement part emits slightly brighter light (Figure 3e).

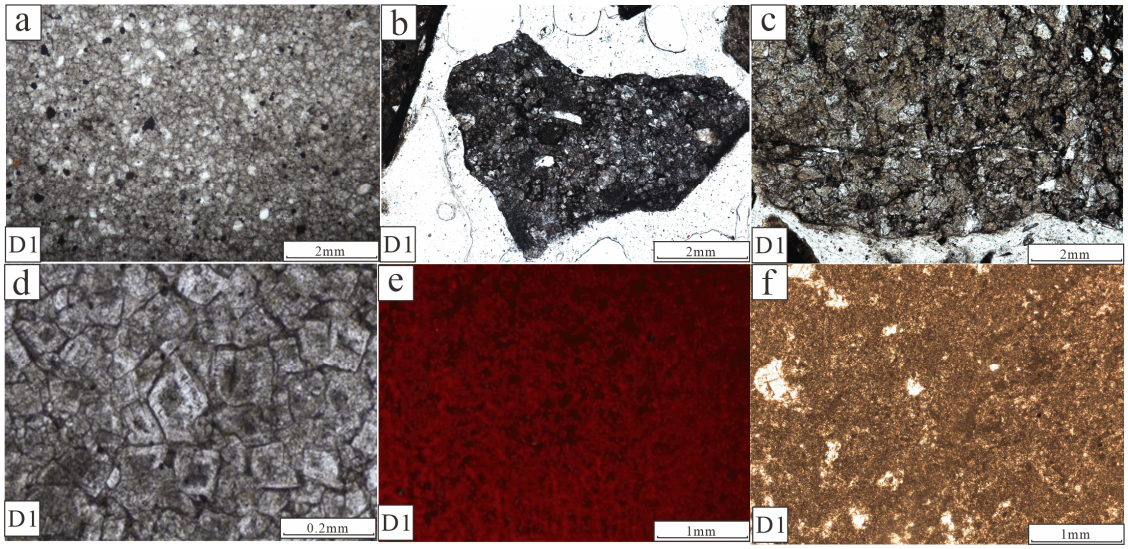

Figure 2. Central–northern Sichuan Cang-1 Member D1 reservoir lithologic characteristics. (**a**) Fine crystalline dolostone, dominated by crystalline texture; dolomite crystals subhedral and in mosaic contact, 10×, plane-polarized light (–), MX202 well, 4730.16 m; (**b**) silt crystalline dolostone, with minor silt content, 50×, plane-polarized light (–), JT1 well, 6965 m; (**c**) silt crystalline dolostone, exhibiting a "dirty" brownish hue, 50×, plane-polarized light (–), JT1 well, 6987 m; (**d**) silt crystalline dolostone, showing recrystallization, with cloudy-core–bright-rim texture, 10×, plane-polarized light (–), MX202 well, 4727 m; (**e**) silt crystalline dolostone, exhibiting a dull and uniform red luminescence under cathodoluminescence, 2.5×, MX17 well, 4680.6 m; (**f**) silt crystalline intraclastic dolostone, cemented by sparry dolomite, 2.5×, plane-polarized light (–), CT1well, 5930.97 m.

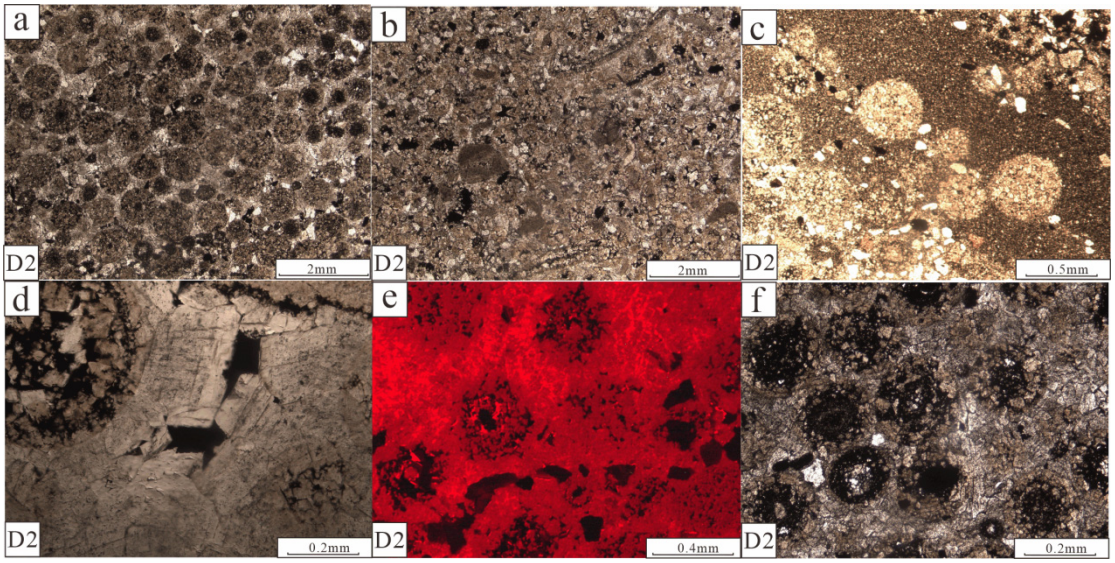

Figure 3. Central–northern Sichuan Cang-1 Member D2 reservoir lithologic characteristics. (**a**) Terrigenous quartz-bearing intraclastic oolitic dolostone, plane-polarized light (–), CT1 well, 6271.75 m; (**b**) intraclastic oolitic bioclastic dolostone, plane-polarized light (–), CT1 well, 6273.77 m; (**c**) oolitic dolostone, ooid cores and concentric laminae composed of euhedral to subhedral silt-to-fine crystalline dolomite, plane-polarized light (–), CT1 well, 6271.32 m; (**d**) oolitic dolostone, with intercrystalline pores filled by bitumen; plane-polarized light (–), CT1 well, 6267.33 m; (**e**) oolitic dolostone, ooids exhibit weak dull-red cathodoluminescence, while the cement phase shows slightly brighter luminescence, CT1 well, 6261.25 m; (**f**) oolitic dolostone with selective dissolution generating intragranular dissolution pores that are subsequently filled by bitumen.

(3) Residual Textured Dolomite (D3)

D3 is widely developed in the northern Sichuan region. The hand specimen color is mainly flesh-red. Under the microscope, it can be distinguished from D2 by bioclasts (Figure 4a), psammite ghosts (Figure 4b), outlines, and shadows. It is mainly composed of xenomorphic medium-coarse crystalline dolomite with relatively turbid crystals and partially preserved granular textures (Figure 4c). A type of dolomite, which is mostly formed by the dolomitization of limestone during the diagenetic stage, is widely distributed in the study interval. Therefore, D3 mostly retains its crystal morphology and size before replacement. However, due to compaction and dissolution, some dissolution fractures and stylolites cutting through the original grains can be observed (Figure 4d), which are filled with gypsum cements or organic matter; dolomite emits orange–red-to-red luminescence under cathodoluminescence (Figure 4e).

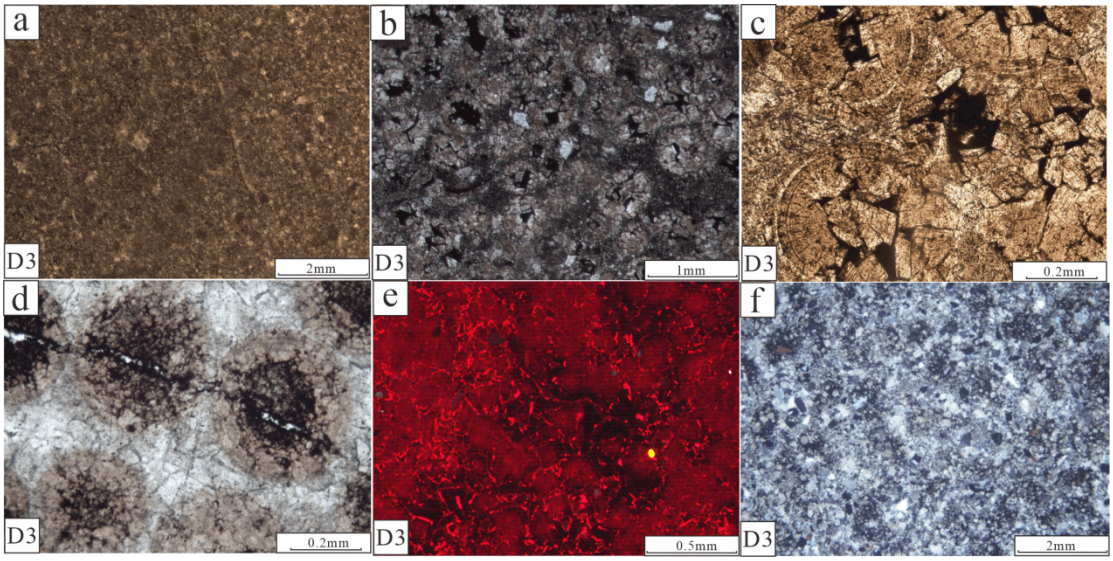

Figure 4. Central–northern Sichuan Cang-1 Member D3 reservoir lithologic characteristics. (**a**) Relict silt crystalline dolostone, exhibiting ghost texture of precursor grains, 1.25×, plane-polarized light (–), CT1 well, 5905.31 m; (**b**) relict intraclastic oolitic dolostone, plane-polarized light (–), CT1 well, 6273.21 m; (**c**) medium crystalline dolostone, with relic oolitic texture, 5×, plane-polarized light (–), CT1 well, 6267 m; (**d**) relict oolitic dolostone, ooids filled with bitumen, dissolution seams cross-cutting ooids visible, 10×, plane-polarized light (–), CT1 well, 6194.36 m; (**e**) Relict fine crystalline dolostone, dolomite exhibits orange–red-to-red cathodoluminescence, CT1 well, 6257.33 m; (**f**) relict oolitic dolostone, intensely recrystallized, relicooids composed of fine to silt crystalline dolomite and bitumen; 4×, plane-polarized light (–), CT1 well, 6173.56 m.

4.2. Reservoir Characteristics

4.2.1. Reservoir Space Types

After long-term geological evolution, the reservoir space types of the Cang-1 Member in the study area are complex, constrained by various diagenetic processes and influenced by tectonic activities [51,52]. Based on core observation, the reservoir spaces of the Cang-1 Member are classified into three categories (pores, fractures, and vugs) according to their size, morphology, genesis, and relationship with rock texture.

(1) Pores

Pores are the most dominant reservoir space type in the study area. According to their genesis and morphology, they can be subdivided into intercrystalline pores, intergranular pores, and intragranular pores. Intercrystalline pores are commonly found in D1 with relatively large grains, which are mostly formed by recrystallization. In addition,

intercrystalline pores also include residual reservoir spaces in dissolution pores after extensive filling by cementing minerals. These intercrystalline dissolution pores are generally distributed near fluid migration pathways such as fractures and pressure solution seams (Figure 5a). Intergranular pores are mainly developed in D2 but are mostly damaged, filled by multi-stage cementation, or transformed into intergranular dissolution pores through multi-stage dissolution (Figure 5b). They are also a major reservoir space type in the study area. Intragranular dissolution pores are formed by selective dissolution within crystals or grains. Microscopic observation shows that intragranular dissolution pores are mainly distributed in some bioclasts and residual ooids (Figure 5c) and are also a common pore type.

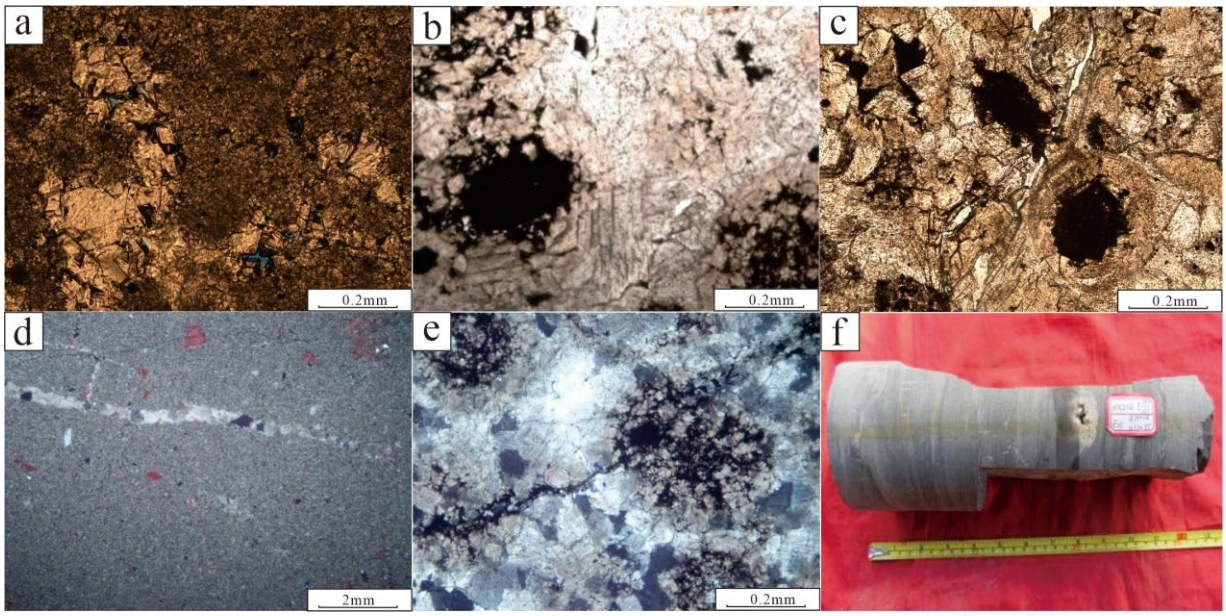

Figure 5. Reservoir space characteristics of the Cang-1 Member in central–northern Sichuan Basin. (**a**) Sandy silt crystalline dolostone with well-developed intercrystalline and relic intercrystalline pores, 10×, plane-polarized light (–), CT1 well, 5943.4 m; (**b**) oolitic dolostone, residual intergranular pores filled by bitumen, 40×, plane-polarized light (–), CT1 well, 6014.36 m; (**c**) oolitic dolostone, dolomite-cemented, residual intragranular pores filled by bitumen; plane-polarized light (–), CT1 well, 6273.33 m; (**d**) calcareous fine silt crystalline dolostone, one diagenetic micro-fracture filled by dolomite, 4×, crossed nicols (+), BL1 well, 5836.5 m; (**e**) Relict oolitic dolostone, relic ooids filled by bitumen, dissolution seams visible, 10×, plane-polarized light (–), CT1 well, 6094.21 m; (**f**) Grey silt crystalline dolostone, vuggy pore (dissolution cavern), MX202 well, 4730.3 m.

(2) Fractures

Fractures are reservoir spaces formed by rock fragmentation under stress, including structural fractures, dissolution fractures, and pressure solution seams [53–55]. In addition to serving as reservoir spaces, fractures can significantly improve reservoir permeability, facilitating fluid flow within the reservoir [56–58]. The Canglangpu Formation in the study area has experienced multiple tectonic cycles, developing various types of multi-stage fractures. Some fractures are filled with different minerals such as dolomite and calcite. Under microscopic observation, fractures are classified by genesis into diagenetic fractures (Figure 5d), structural fractures, and dissolution fractures developed along existing fractures, which are filled with organic-rich argillaceous materials. Another type of diagenetic fracture is characterized by dissolution along the fracture plane and is relatively narrow. Structural fractures in the rock are often straight and filled with late-stage authigenic minerals such as pyrite. Most dissolution fractures develop from pre-existing fractures

through dissolution, typically appearing curved and irregular, and are also filled in the later stage [59–62] (Figure 5e).

(3) Cavity

A cavity refers to a dissolution space with a diameter greater than 2 mm. Its formation process is similar to that of dissolved pores, but cavities are larger in size and scale compared with dissolved pores. Cavities are well-developed in the central Sichuan area, showing full filling or partial filling characteristics (Figure 5f).

In summary, the pore development in the three types of reservoir rocks is primarily controlled by the pore network inherited from their original sedimentary texture and the intensity of post-depositional diagenetic alterations, particularly cementation, dissolution, and compaction [53]. Among them, D2 exhibits the best reservoir quality due to its well-preserved primary intergranular pores. D3 ranks second, as its pore system relies mainly on late-stage dissolution seams that are often extensively filled. In contrast, D1 shows the poorest porosity owing to recrystallization-induced densification and the general lack of effective pore spaces.

4.2.2. Reservoir Physical Properties

Based on the logging physical property data of multiple wells (Chongtan 1, Gaoshi 10, Guangtan 2, Jiaotan 1, etc.) in the Canglangpu Formation, the reservoir development of the Cang-1 Member in the study area was analyzed. The results show that the Cang-1 Member has low porosity: the average porosity of each well does not exceed 5%, with a distribution range of 2.52% to 4.70% and an average value of 3.63% (Figure 6a), belonging to a low-porosity reservoir [45,52,63]. Analysis of the permeability data from multiple wells (Chuanshen 1, Gaoshi 10, Guangtan 2, etc.) in the Cang-1 Member indicates that the permeability ranges from 0.005×10^{-3} mD to 0.12×10^{-3} mD. As shown in the figure, the Jiaotan 1 and Chuanshen 1 wells have relatively high permeability, while other wells have low permeability (all less than 0.02×10^{-3} mD) (Figure 6b).

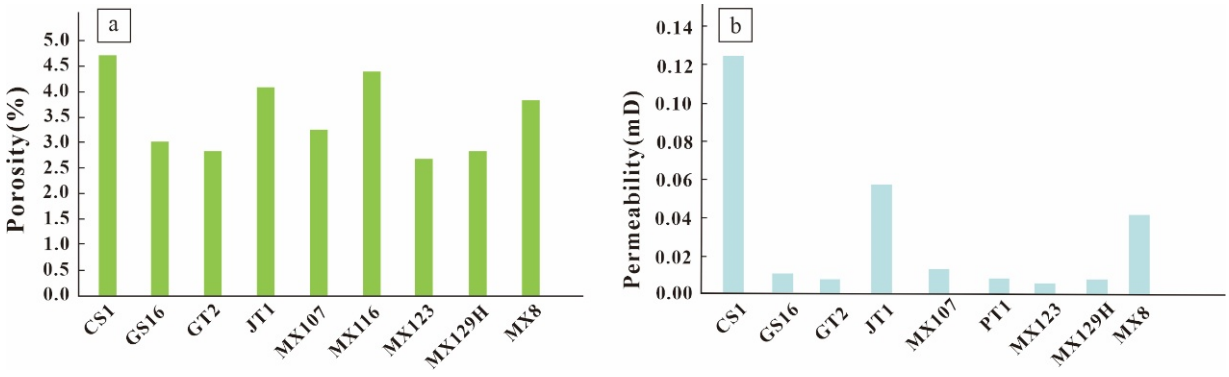

Figure 6. Reservoir physical property profile of the Cang-1 Member, central–northern Sichuan Basin. (**a**) Porosity characteristics of the Cang-1 Member reservoir, central–northern Sichuan. (**b**) Permeability characteristics of the Cang-1 Member reservoir, central–northern Sichuan Basin.

The porosity–permeability cross plot of the Cang-1 Member reveals a weak positive correlation between porosity and permeability, indicating that pore throats still have a significant impact on reservoir seepage capacity (Figure 7). The reservoir is generally classified as a fracture porosity type, which is consistent with the relatively high permeability of the Chuanshen 1 and Chongtan 1 wells. Meanwhile, the porosity–permeability relationship of gas logging intervals was discussed to determine the lower limits of porosity and permeability for the Cang-1 Member reservoir. The results show that for wells with gas logging in the Canglangpu Formation, the porosity is greater than 2% (and greater than 3%

for gas pay zones). Permeability is positively correlated with porosity, and the permeability of gas pay zones is generally greater than 0.02 × 10^{-3} mD (Figure 7).

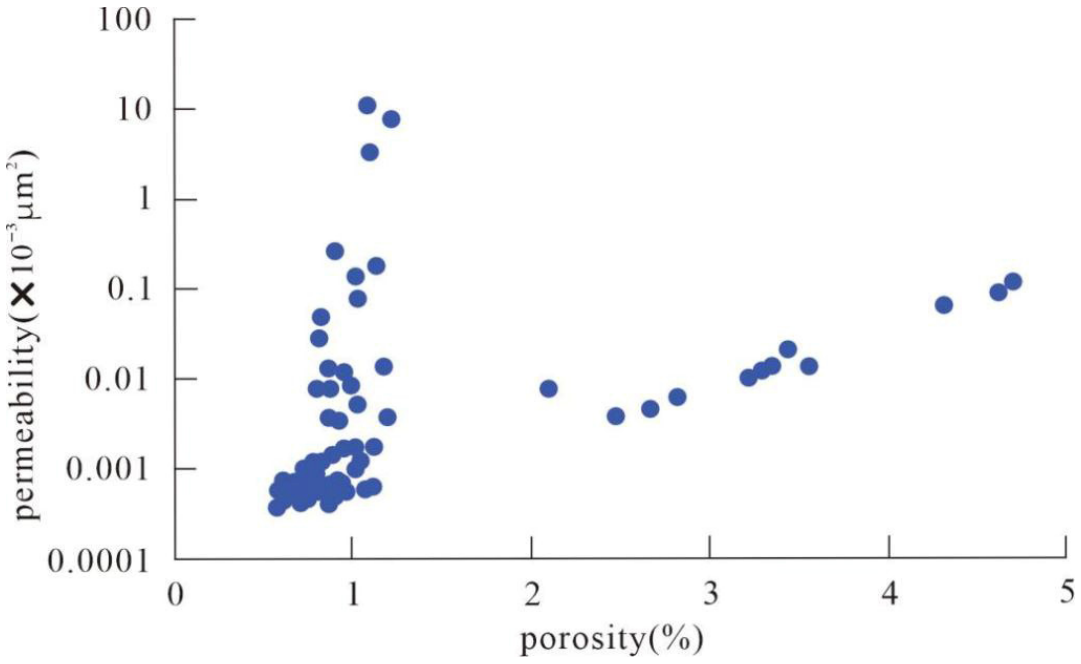

Figure 7. Porosity–permeability cross-plot for the Cang-1 Member reservoir, central–northern Sichuan Basin.

4.3. Geochemical Characteristics

4.3.1. Carbon and Oxygen Isotope Characteristics

In this study, whole-rock carbon and oxygen isotope analysis was conducted on dolomite samples from the Cang-1 Member in the Sichuan Basin, and abnormal data points ($\delta^{18}O < -10‰$ (PDB), $\delta^{13}C < -2.5‰$ (PDB)) were excluded [46,64,65]. On this basis, the paleosalinity Z-value and diagenetic temperature were calculated, and the test results are as follows: the $\delta^{13}C$ values of D1 range from −2.1‰ to −1.5‰, and the $\delta^{18}O$ values range from −9.2‰ to −7.8‰ (Figure 8), which fall within the range of $\delta^{13}C$ (−2.5‰~2.0‰ V-PDB) and $\delta^{18}O$ (−10~−7‰ V-PDB) of coeval seawater during the Cambrian [66], with paleosalinity Z-values of 118~120; the $\delta^{13}C$ values of D2 range from −1.8‰ to −0.9‰ and the $\delta^{18}O$ values range from −8.1‰ to −6.5‰ (Figure 8), which are basically consistent with the range of coeval Cambrian seawater, with paleosalinity Z-values of 120~122; the $\delta^{13}C$ values of D3 range from −2.1‰ to 0.4‰ and the $\delta^{18}O$ values range from −9.8‰ to −7.6‰ (Figure 8), which are within the same range as coeval Cambrian seawater, with paleosalinity Z-values of 122~125. Overall, the paleosalinity Z-values range from 106.72 to 125.10, with an average of 120.76, and the diagenetic temperatures calculated based on isotope data range from 16.6 °C to 38.7 °C, with an average of 27.25 °C.

4.3.2. Strontium Isotope Characteristics

The $^{87}Sr/^{86}Sr$ ratios of D1 in the Cang-1 Member from the central–northern Sichuan Basin range from 0.7108 to 0.7120, with an average of 0.7114, which is higher than the range of $^{87}Sr/^{86}Sr$ ratios of coeval Cambrian seawater (0.7075–0.7095) [67–69] (Figure 9). The $^{87}Sr/^{86}Sr$ ratios of D2 range from 0.7098 to 0.7110, with an average of 0.7104, while those of D3 range from 0.7095 to 0.7102, with an average of 0.7098 (Figure 9). The strontium isotope distributions of the three types of dolomites in the study area show a wide range, and there are differences in the deviations between the ratios of different lithologies and seawater.

Most samples have strontium isotope ratios slightly higher than the range of Cambrian seawater strontium isotopes (Figure 9).

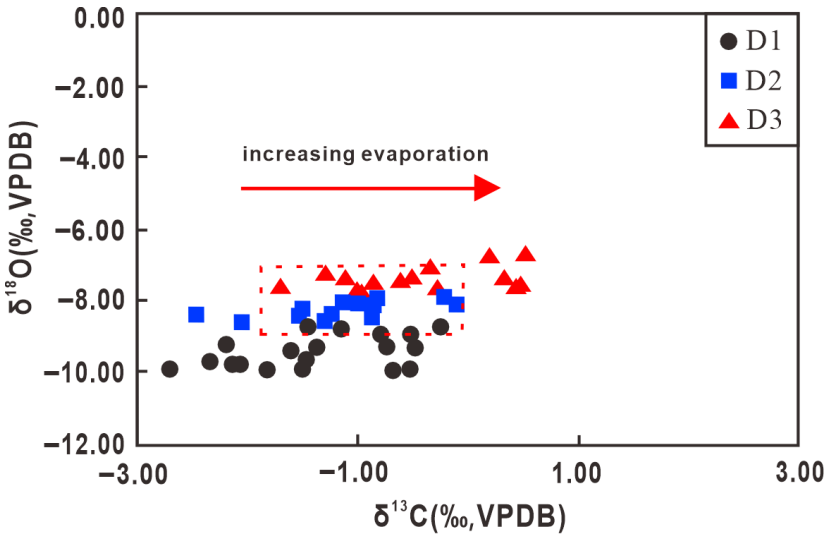

Figure 8. Carbon and oxygen isotope signature of the Cang-1 Member reservoir, central–northern Sichuan Basin.

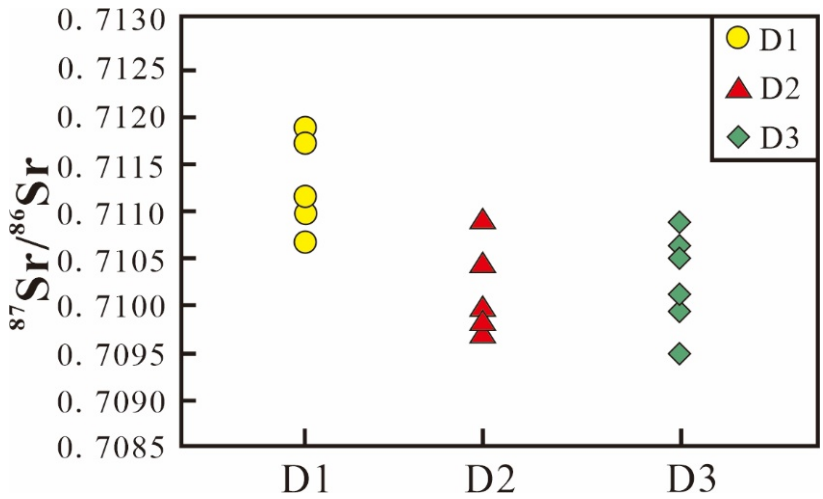

Figure 9. Strontium isotope signature map of the Cang-1 Member reservoir, central–northern Sichuan Basin.

4.3.3. X-Ray Diffraction Order Degree Analysis of Dolomite

Among the three types of dolomites in the study area, the order degree of D1 ranges from 0.46 to 0.50, with an average of 0.49, that of D2 ranges from 0.64 to 0.69, with an average of 0.67, and that of D3 ranges from 0.70 to 0.82, with an average of 0.77, and the average ordering degree of dolomite is 0.64. The order degree values of all dolomite samples range from 0.46 to 0.82 without abnormally discrete data, and there are significant differences in order degree among different lithologies. Overall, the order degree increases with the increase in dolomite grain size, and the crystal structure gradually tends to be ideal [46,67] (Table 1).

Table 1. Orderliness characteristics of different types of dolomite in the study area.

Well No.	Lithology	Depth (m)	Ordering Degree	Mean Value	
CT1	D1	6258.5	0.50	0.49	0.64
CT1	D1	6270	0.49		
CT1	D1	6288.65	0.50		
BL1	D1	5075	0.46		
CT1	D2	6310	0.66	0.67	
CT1	D2	6315.72	0.67		
CT1	D2	6322	0.64		
MX202	D2	4780	0.67		
MX202	D2	4795	0.68		
GS10	D2	4806.4	0.69		
CT1	D3	6338	0.76	0.77	
MX202	D3	4800	0.75		
GS10	D3	4822	0.82		
GS10	D3	4839.1	0.77		
GS10	D3	4855.32	0.70		
GS10	D3	4860	0.79		

5. Discussion

5.1. Constraints of Geochemical Indicators on the Genesis of Dolomite Reservoirs

The three types of dolomites in the study area share similar dolomitization fluid characteristics, with fluids derived from Lower Cambrian seawater. The following is a detailed discussion on the supporting evidence and characteristics of geochemical indicators for the origin of dolomitization fluids in the three types of dolomites.

Carbon isotopes are relatively stable in dolomites and may only change after intense diagenesis, such as dolomitization related to organic matter degradation and hydrothermal activity [70]. In contrast, oxygen isotopes are more sensitive and prone to alteration by changes in diagenetic temperature, evaporation, and meteoric water leaching [71]. D1 is mostly developed in the upper part of the Cang-1 Member, and most studies have shown that the formation of D1 is mainly related to penecontemporaneous dolomitization of surface seawater [72,73]. The $\delta^{13}C$ and $\delta^{18}O$ values of D1 (−2.1‰~−1.5‰, −9.2‰~−7.8‰) fall entirely within the range of Lower Cambrian seawater calcite precipitates ($\delta^{13}C$: −2.5‰~2.0‰ V-PDB; $\delta^{18}O$: −10‰~−7‰ V-PDB), indicating that the dolomitization fluid was dominated by penecontemporaneous seawater. Strontium isotope research can serve as a key parameter for fluid origin, primarily because Sr isotopes do not fractionate due to temperature, pressure, or microbial activity [56,73] and can directly reflect the isotopic composition of the fluid. Additionally, the residence time of Sr in seawater is much longer than the seawater mixing time, resulting in a homogeneous isotopic composition of marine Sr globally during any geological period [53,74]. The $^{87}Sr/^{86}Sr$ ratios of D1 range from 0.7108 to 0.7120, which are generally higher than the Sr isotope range of Cambrian seawater (0.7075–0.7095). A geochemical phenomenon that may stem from the input of terrigenous clastics rich in ^{87}Sr during the formation of D1 is associated with sea level fall, which promoted the input of terrigenous Sr and thus induced an increase in the ratio [44,75]. Furthermore, D1 has a low order degree, with an average of 0.49, indicating rapid crystal growth. Its cathodoluminescence characteristics are weak-to-dim,

suggesting that such rocks were mostly formed in a hypersaline tidal flat environment with strong evaporation [76], which is consistent with the conclusion that D1 formed under near-surface conditions.

The order degree ranges of D2 and D3 are 0.64~0.69 and 0.70~0.82, respectively, indicating that both types of dolomites grew relatively slowly with sufficient time to form ordered dolomite lattices and high crystallization degrees. They may have undergone recrystallization (Figure 4f) or burial dolomitization during the burial process [77,78]. Diagenetic temperature and pressure increase with burial depth, and recrystallization in shallow-to-medium burial environments makes dolomite crystal arrangement more ordered, improves the connectivity of intercrystalline pores, and further optimizes reservoir seepage capacity [64,78]. The $\delta^{13}C$ values of D2 range from −1.8‰ to −0.9‰ and $\delta^{18}O$ values from −8.1‰ to −6.5‰, while the $\delta^{13}C$ values of D3 range from −2.1‰ to 0.4‰ and $\delta^{18}O$ values from −9.8‰ to −7.6‰. Among these, the $\delta^{13}C$ values are basically consistent with the range of coeval Cambrian seawater, and the $\delta^{18}O$ values are higher than those of coeval seawater, which may be caused by the input of terrigenous clastics [34,53,79]. The $^{87}Sr/^{86}Sr$ ratios of D2 range from 0.7098 to 0.7110, and those of D3 range from 0.7095 to 0.7102, both slightly higher than the Sr isotope range of Cambrian seawater. This may be due to the proximity to the northern Sichuan area and ancient land, leading to increased terrigenous input, or the modification by secondary dolomitization fluids during the late diagenetic process. It reveals that Sr with high radiogenic origin may have been involved in the dolomitization process with increasing burial [65,80]. The Z-values of D1 and D2 are both around 120 (note, the original text mentions "120 °C", which is logically inconsistent with the paleosalinity Z-value; it has been corrected to consistent numerical expression), slightly higher than normal seawater, indicating that the diagenetic fluid had high salinity. This suggests that the parent rock of dolomitization was limestone, and the dolomitization fluid was still dominated by high-salinity concentrated coeval seawater [60].

The geochemical characteristics further reveal the fluid environment and diagenetic intensity for the formation of dolomite reservoirs in the study area, indicating that the three types of dolomites in the study area were mainly formed in a marine-derived fluid environment during the penecontemporaneous period and shallow burial stage.

5.2. Main Controlling Factors of Reservoir Development

The formation and distribution of the Cang-1 Member reservoir are influenced and constrained by multiple factors. Based on the evolutionary characteristics of sedimentation, diagenesis, and tectonism in the platform margin belt of the Penglai Gas Field, central Sichuan paleouplift, sedimentary facies belts provide the material basis for reservoir development. Constructive diagenesis represented by karstification controls the formation of high-quality reservoirs, while tectonism improves the scale of high-quality reservoirs.

5.2.1. Sedimentary Facies on Reservoir Development

Lithology controls the development of sedimentary facies, and sedimentary facies belts determine the initial material basis and primary porosity development potential of reservoirs [81]. From the perspective of petrological characteristics, D2—the high-quality reservoir rock type in the study area—is mainly developed in the grain bank microfacies of carbonate shallow-water shelves (e.g., the top of the Cang-1 Member in the Gaoshi–Moxi area). Within this facies belt, grains (oolites, sand clasts, bioclasts) have good sorting and rounding, with initially developed primary intergranular pores (the surface porosity can reach 3%~5%), providing a spatial basis for later diagenetic modification. In contrast, D1 is mainly developed in lagoon or tidal flat facies with low energy, where primary porosity is underdeveloped (surface porosity < 1%) and is prone to further destruction by compaction–

pressure dissolution. However, its reservoir performance can be gradually improved through the modification of late diagenetic fluids [66,82]. Combined with the distribution law of sedimentary facies (the grain banks of the Cang-1 Member are distributed in a zonal pattern along the high parts of the central Sichuan paleouplift), it is confirmed that the paleogeomorphic pattern of "local uplifts controlling banks" is a prerequisite for the development of high-quality reservoirs. The high parts of the paleouplift had strong water energy [83], which was conducive to grain enrichment and the formation of rigid frameworks, alleviating the destruction of pores by later compaction [47,82].

5.2.2. Diagenesis on Reservoir Development

Diagenesis exerts significant constructive and destructive effects on reservoir physical properties, with distinct differences in its impacts across various diagenetic stages. The target interval investigated in this study is the Canglangpu Formation, primarily focusing on Member 1 of the Canglangpu Formation. Herein, we mainly discuss the constructive diagenesis that favors the formation of high-quality reservoirs within Member 1 of the Canglangpu Formation.

Dissolution refers to the process where certain chemical components (or minerals) in sediments or sedimentary rocks are dissolved and enter the solution under specific physical and chemical conditions [34,84]. Based on the stages of diagenesis and differences in dissolution targets in carbonate rocks, it can be divided into selective dissolution during the eodiagenetic stage, and non-selective dissolution during the mesodiagenetic and burial diagenetic stages [78,81]. During the eodiagenetic stage, D2 undergoes selective dissolution to form intragranular dissolved pores or moldic pores. Most of these pores are later filled with dolomite and asphalt, resulting in residual intragranular dissolved pores (Figure 3f). Non-selective dissolution during the mesodiagenetic and burial diagenetic stages is based on structural fractures and pre-existing pores. Fluids flow along fracture–vug systems, expanding the original pores or fractures into intercrystalline dissolved pores and dissolved fractures. According to the asphalt filling status, the dissolved vugs can be divided into those formed earlier than and later than hydrocarbon charging [78] (Figure 9).

Penecontemporaneous dolomitization laid the foundation for the development of intercrystalline pores in D1, and dolomitization during the eodiagenetic stage can increase porosity by 2%~3%. Tectonic fracturing caused by tectonic movements generates high-angle structural fractures that can connect isolated dissolved pores, forming a "pore–fracture" system and increasing permeability by 1~2 orders of magnitude (Figure 10). This is consistent with the relatively high $^{87}Sr/^{86}Sr$ ratios of D3 (0.7095~0.7102) in geochemical characteristics, which indicates the result of late-stage fluid modification. Hydrocarbon charging allows organic matter to enter pores early, effectively preventing the migration of dissolved substances and inhibiting the occurrence of chemical compaction [63,85]. Hydrocarbon filling in pores can effectively suppress cementation and metasomatism, thus preserving the secondary pores formed in the early stage. The hydrocarbons formed in the late stage can also promote the expansion of pore volumes occupied by hydrocarbons, thereby displacing formation water and reducing the probability of water–rock reactions [66,86]. Furthermore, crude oil cracking is usually accompanied by overpressure formation, and abnormal fluid pressure plays a role in dissolving and protecting the previously formed secondary pores of the reservoir, while inhibiting further compaction [50,87].

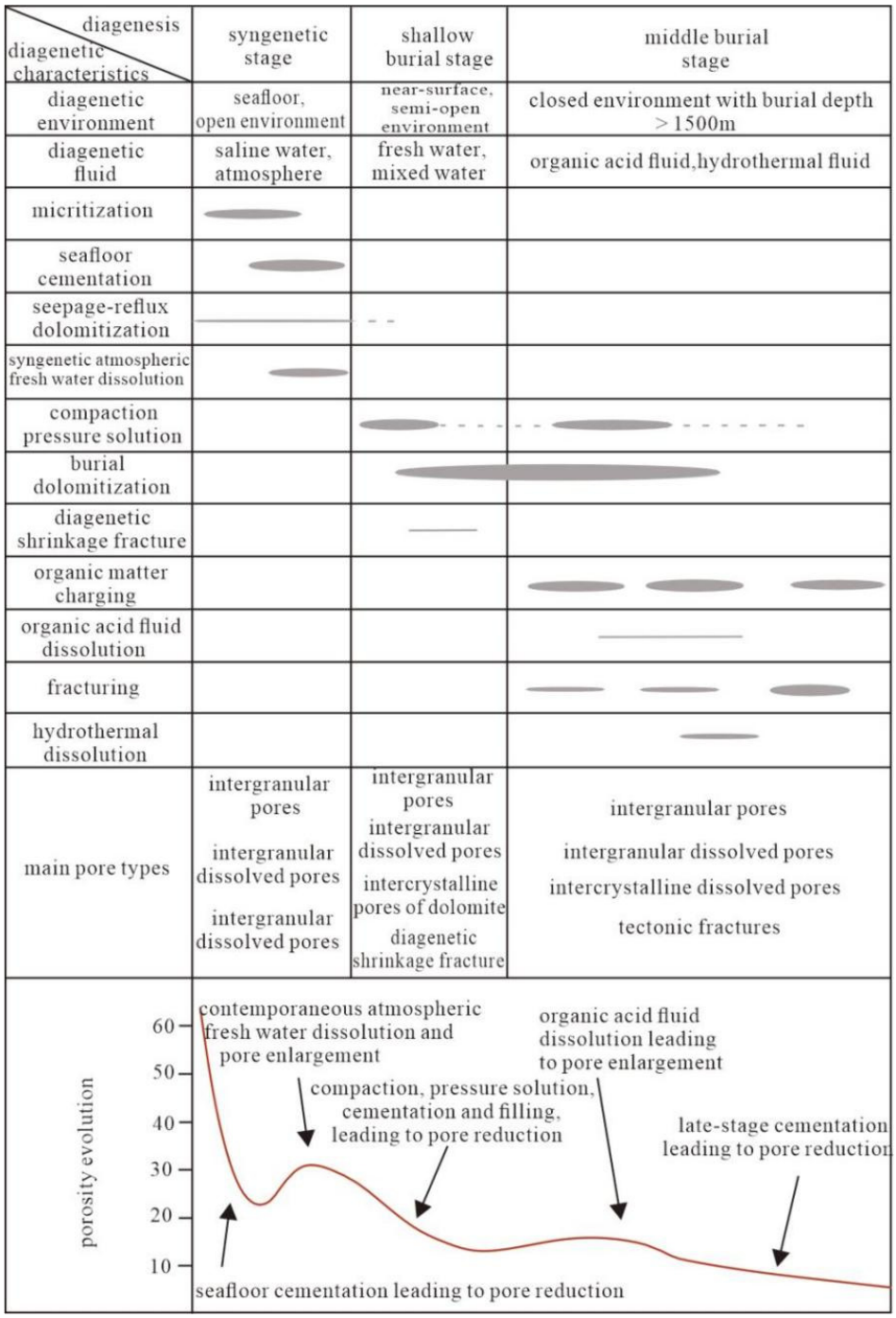

Figure 10. Diagenetic sequence chart of the Cang-1 Member Reservoir, central–northern Sichuan Basin [46].

5.2.3. Tectonism on Reservoir Development

The Cambrian strata in the study area have been modified by multiple phases of tectonism. In particular, the fractures formed during the Caledonian and Hercynian tectonic movements have exerted a significant impact on hydrothermal migration and greatly improved reservoir physical properties [32,54,88]. However, with the progression of diagenesis, most fractures have been filled with later-formed asphalt, calcite, and dolomite—though the formation of fractures effectively enhanced rock permeability at the time of their generation [82,86].

During the early sedimentary stage of the Canglangpu Formation, the Mianyang–Changning Rift Trough was not filled, preventing terrigenous clastic materials from the Kangdian, Luding, and Motianling ancient lands from being transported to the areas east of the rift trough [89]. The sedimentary environment of the study area was dominated by carbonate deposition. Meanwhile, with sea level rise and water depth increase, dolomite deposition developed in the structural high areas [5]. Overall, the distribution of early dolomite was mainly affected by the unfilled Mianyang–Changning Rift Trough, which hindered the supply of terrigenous clastic materials from the Kangdian, Luding, and Motianling ancient lands to the areas east of the rift trough. This resulted in a shallow-water sedimentary environment in the central Sichuan area, promoting the formation of dolomite [38,90].

During the late sedimentary stage of the Canglangpu Formation, the Mianyang–Changning Rift Trough was fully filled and leveled. The Hannan ancient land was uplifted to the surface, and with the rise in sea level and increase in water depth, a large amount of terrigenous clastic materials were transported from the ancient lands around the basin to the interior of the basin. This resulted in a restricted distribution of dolomite deposition in the Sichuan Basin [63,75], which only developed in the Ziyang–Weiyuan and Moxi areas within the Leshan–Longnüsi paleouplift. This is mainly because the area is located at a relatively high structural position with shallow water depth, and the northern and southern flanks of the paleouplift hindered the supply of terrigenous clastic materials from the ancient lands to a certain extent [51,91].

5.3. Reservoir Formation Mechanism and Development Model

During the deposition of the first member of the Canglangpu Formation (Cang-1 Member) in the study area, the sedimentary setting inherited that of the Qiongzhusi Formation [32,47,92]. Sea level fluctuated significantly, and provenance from the Kangdian ancient land continuously migrated toward the basin interior. Influenced by the Deyang–Anyue ancient rift, a large amount of clastic rocks filled the rift, resulting in a substantial reduction in clastic supply to the basin interior. The basin interior was dominated by carbonate deposition, accompanied by some mixed clastics, developing carbonate shallow-water shelf facies and grain bank microfacies [45,87]. Primary porosity was well-developed, which was conducive to later dolomitization and provided a sufficient material basis (Figure 11a). During the deposition of the second member of the Canglangpu Formation (Cang-2 Member), extensive regression led to the predominant development of tidal flat facies and clastic shallow-water shelf facies. Therefore, reservoir development during the Canglangpu period was controlled by sedimentary facies, mainly distributed in the basin interior and concentrated in the central Sichuan and northern slope areas [63,73,84](Figure 11b).

During the burial period of the Canglangpu Formation, the early-deposited limestone grain banks began to undergo dolomitization and were gradually transformed into oolitic dolomites of dolomitized grain bank facies. However, differences in burial depth led to differential dolomitization. Overall, the northern slope of the central Sichuan area had a greater burial depth, where dolomitization was more intensive [63,87,90]. Correspondingly, intercrystalline pores and dissolved pores were well-developed, resulting in better reservoir quality. Meanwhile, tectonism also influenced reservoir development: rock fracturing caused by tectonic activities formed fracture-type pores, which improved reservoir quality and expanded the scale of reservoir development [46,59,65] (Figure 11c).

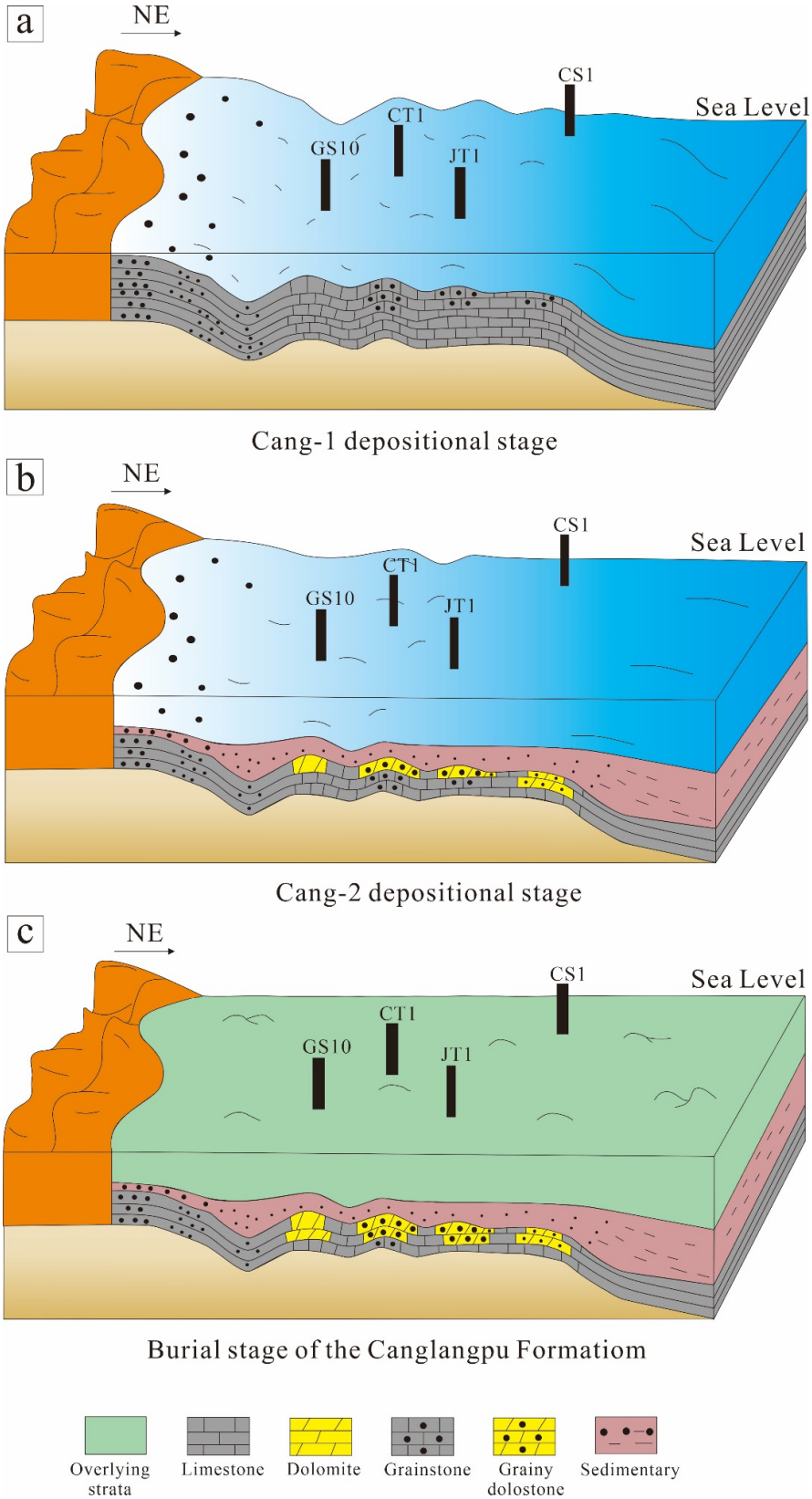

Figure 11. Reservoir development model of the Canglangpu Formation, central–northern Sichuan Basin. (**a**) Cang-1 Member sedimentary period. (**b**) Cang-2 Member sedimentary period. (**c**) Burial stage of the Canglangpu Formation.

6. Conclusions

This study focuses on the Cambrian Canglangpu Formation dolomites in the central–northern Sichuan Basin. Based on macro- and microscopic petrological characteristics, a systematic classification scheme for dolomites is proposed. The types and sources of diagenetic fluids involved in dolomitization are traced, and the controlling factors for the development of dolomite reservoirs are clarified. The main conclusions are summarized as follows:

(1) Based on a comprehensive study of field section measurement, drilling core observation, reservoir characteristics, and geochemical analysis of the Cambrian Canglangpu Formation dolomite reservoirs in the central–northern Sichuan area of the Sichuan Basin, the dolomites of the Cang-1 Member in this area are uniformly classified into three types: D1 is fine- to very fine-grained dolomite, D2 is granular dolomite, and D3 is relict-textured dolomite. The reservoir spaces are mainly intercrystalline pores, intergranular pores, and structural fractures, among which D2 has the best reservoir physical properties.

(2) Geochemical characteristics reveal the fluid environment and diagenetic background for reservoir formation. D1 was mainly formed in a hypersaline tidal flat environment with intense evaporation under near-surface penecontemporaneous seawater conditions. Based on the order degree values, D2 and D3 were formed through burial and recrystallization. Furthermore, by analyzing the $\delta^{13}C$, $\delta^{18}O$, and $^{87}Sr/^{86}Sr$ ratios, it is concluded that D2 and D3 were primarily formed during the shallow-to-medium burial stage by coeval high-salinity concentrated seawater via reflux seepage.

(3) The development of dolomite reservoirs is jointly controlled by three factors: "sedimentation–diagenesis–tectonism". Sedimentary facies belts are the foundation—the grain bank microfacies of carbonate shallow-water shelves provide high-quality material basis and primary porosity potential for reservoirs. Diagenesis is the key—reflux dolomitization lays the foundation for reservoir spaces, and organic acid dissolution during the middle-deep burial stage is the core for the formation of high-quality reservoirs. Tectonism is the optimization—Caledonian–Hercynian tectonic fractures effectively connect isolated pores, significantly improving reservoir permeability. The coupling of these three factors forms the genetic mechanism of high-quality reservoirs characterized by "sedimentation laying the foundation, diagenesis modifying, and tectonism optimizing".

Author Contributions: Conceptualization, F.H., X.W. and Z.X.; Methodology, Y.H.; Validation, F.H.; Investigation, X.W. and Z.X.; Data curation, Z.W. (Zhun Wang) and B.L.; Writing—original draft, C.H. and X.W.; Writing—review & editing, Z.W. (Zhengdong Wang) and K.L.; Visualization, F.H. and C.H.; Supervision, F.H.; Funding acquisition, F.H. All authors have read and agreed to the published version of the manuscript.

Funding: This research was funded by The orderly distribution pattern of conventional and unconventional oil and gas in the Shizhou System—Middle Triassic section and the selection of potential reservoir areas for reservoir expansion grant number 2025ZD1400403 And The APC was funded by SINOPEC Key Laboratory of Petroleum Accumulation Mechanisms, Wuxi.

Data Availability Statement: The original contributions presented in this study are included in the article. Further inquiries can be directed to the corresponding author.

Conflicts of Interest: The authors declare no conflict of interest.

References

1. Shen, A.J.; Luo, X.Y.; Hu, A.P.; Qiao, Z.F.; Zhang, J. Dolomitization pathways from penecontemporaneous to burial environments and their reservoir-forming effects. *Pet. Explor. Dev.* **2022**, *49*, 731–743. [CrossRef]
2. Wang, G.Z.; Liu, S.G.; Li, N.; Wang, D.; Gao, Y. Formation and preservation mechanisms of high-quality reservoirs in deeply buried dolomites of the Dengying Formation, northern margin of the Sichuan Basin. *Acta Petrol. Sin.* **2014**, *30*, 667–678.
3. Han, D.K.; Fu, H.; Liu, Y.T. Influence of dolomitization on reservoir development of the Changxing Formation in the Yuanba area. *Nat. Gas Ind.* **2011**, *31*, 22–26.
4. Wang, Y.P.; Bao, Z.D.; Zhang, L.J.; Yang, D.F.; Wen, W.; Zhong, Y.; Tang, P. Diagenesis of microbialite reservoirs in the second member of the Ediacaran Dengying Formation in the Penglai area, Sichuan Basin: Implications for the formation and evolution of high-quality reservoirs. *J. Geomech.* **2024**, *30*, 579–594.
5. Wen, H.G.; Wen, L.B.; Chen, H.R.; Zheng, R.C.; Dang, L.R.; Li, Y.N. Geochemical characteristics and diagenetic fluids of dolomite reservoirs in the Huanglong Formation, Eastern Sichuan Basin, China. *Pet. Sci.* **2014**, *11*, 52–66. [CrossRef]
6. Zhu, G.Y.; Li, X. Genetic types of dolomite and advances in research methods. *Acta Pet. Sin.* **2023**, *44*, 1167–1190.
7. Warren, J. Dolomite: Occurrence, evolution and economically important associations. *Earth-Sci. Rev.* **2000**, *52*, 1–81. [CrossRef]
8. Vasconcelos, C.; McKenzie, J.A.; Bernasconi, S.; Bernasconi, S.; Grujic, D.; Tiens, A.J. Microbial mediation as a possible mechanism for natural dolomite formation at low temperatures. *Nature* **1995**, *377*, 220–222. [CrossRef]
9. Zhu, G.Y.; Li, X.; Li, T.T.; Zhou, L.; Wu, Y.X.; Shen, B.; Ning, M. Magnesium isotope tracing of dolomitizing fluid migration pathways: A case study of the Carboniferous Huanglong Formation in the Sichuan Basin. *Acta Geol. Sin. (Engl. Ed.)* **2023**, *97*, 753–771.
10. Li, X.; Zhu, G.; Zhang, Z. Genesis of ultra-deep dolostone and controlling factors of large-scale reservoir: A case study of the Sinian Dengying Formation and the Cambrian Longwangmiao Formation in the Sichuan Basin. *Sci. China Earth Sci.* **2024**, *67*, 2352–2382. [CrossRef]
11. Badiozamani, K. The dorag dolomitization model, application to the middle Ordovician of Wisconsin. *J. Sediment. Res.* **1973**, *43*, 965–984. [CrossRef]
12. Adams, J.E.; Rhodes, M.L. Dolomitization by seepage refluxion. *AAPG Bull.* **1960**, *44*, 1912–1920. [CrossRef]
13. Mattes, B.W.; Mountjoy, E.W. *Burial Dolomitization of the Upper Devonian Miette Buildup, Jasper National Park, Alberta*; GeoScienceWorld: Mc Lean, VA, USA, 1980.
14. Koeshidayatullah, A.; Corlett, H.; Stacey, J.; Swart, P.K.; Boyce, A.; Robertson, H.; Whitaker, F.; Hollis, C. Evaluating new fault-controlled hydrothermal dolomitization models: Insights from the Cambrian Dolomite, Western Canadian Sedimentary Basin. *Sedimentology* **2020**, *67*, 2945–2973. [CrossRef]
15. Zhang, J.Q.; Jin, Z.K.; Zhu, X.E.; Li, Y.; Guo, Q.H.; Shi, S.T. Open thermal convection dolomitization: An example from East Yunnan (China). *Geol. Mag.* **2021**, *158*, 330–348. [CrossRef]
16. Zou, C.N.; Du, J.H.; Xu, C.C.; Wang, Z.C.; Zhang, B.M.; Wei, G.Q.; Wang, T.S.; Yao, G.S.; Deng, S.H.; Liu, J.J.; et al. Formation, distribution, resource potential and exploration discoveries of super-large gas fields in the Sinian-Cambrian of the Sichuan Basin. *Pet. Explor. Dev.* **2014**, *41*, 306–325. [CrossRef]
17. Wei, G.Q.; Du, J.H.; Xu, C.C.; Zou, C.N.; Yang, W.; Shen, P.; Xie, Z.Y.; Zhang, J. Characteristics and accumulation models of large gas reservoirs in the Sinian-Cambrian of the Gaoshiti-Moxi area, Sichuan Basin. *Acta Pet. Sin.* **2015**, *36*, 1.
18. Wei, G.Q.; Wang, Z.H.; Li, J.; Yang, W.; Xie, Z.Y. Characteristics, resource potential and exploration directions of Sinian and Cambrian source rocks in the Sichuan Basin. *Nat. Gas Geosci.* **2017**, *28*, 289–302. [CrossRef]
19. Wang, Z.H.; Xie, Z.Y.; Yang, W.; Li, J. Geochemicl characteristics and hydrocarbon—Generating potential of Sinian—CAMBRIAN source rocks in the Sichuan Basin. *Nat. Gas Geosci.* **2017**, *28*, 1–13.
20. Niu, S.Q.; Liu, G.D.; Wang, Y.L.; Song, Z.Z.; Zhu, L.Q.; Zhao, W.Z.; Tian, X.W.; Yang, D.L.; Li, Y.S. Occurrence characteristics and genetic mechanism of pyrobitumen in reservoirs of the Ediacaran Dengying Formation-Cambrian Longwangmiao Formation in the central Sichuan Basin. *Pet. Geol. Exp.* **2024**, *46*, 1039–1049.
21. Wang, X.Q.; Xu, H.; Song, J.R.; Lu, Y.C.; Lu, S.S.; Zhang, H.Y.; Zhang, W.W. Discovery of the Gaoshiti-Longwangmiao giant gas field and petroleum geological characteristics and accumulation of the Sinian-Cambrian in the Sichuan Basin. *Mar. Geol. Front.* **2016**, *32*, 24–32.
22. Jin, M.D.; Zeng, W.; Tan, X.C.; Li, L.; Li, Z.Y.; Luo, B.; Zhang, J.L.; Liu, J.W. Characteristics and controlling factors of beach-controlled karst reservoirs in the Longwangmiao Formation of the Moxi-Gaoshiti area, Sichuan Basin. *Pet. Explor. Dev.* **2014**, *41*, 712–723. [CrossRef]
23. Buggisch, W.; Wang, X.; Alekseev, A.S.; Joachimski, M.M. Carboniferous–Permian carbon isotope stratigraphy of successions from China (Yangtze platform), USA (Kansas) and Russia (moscow Basin and urals). *Palaeogeogr. Palaeoclimatol. Palaeoecol.* **2011**, *301*, 18–38. [CrossRef]
24. Jiang, Q.; Hu, S.; Wang, Z.; Chi, Y.; Yang, Y.; Lu, W.; Li, Q. Paleokarst landform of the weathering crust of Middle Permian Maokou Formation in Sichuan Basin and selection of exploration regions. *Acta Pet. Sin.* **2012**, *33*, 949–960.

25. Zhou, G.; Yang, D.L.; Sun, Y.T.; Yan, W.; Zhang, Y.; Wen, H.G.; He, Y.; Liu, S.B. Sedimentary filling process and petroleum geological significance of the Cambrian Canglangpu Formation in the Sichuan Basin and its surrounding areas. *Lithol. Reserv.* **2024**, *36*, 25–34.
26. Wang, L.; Su, S.T.; Ma, Z.K.; Pu, J.; Yao, L.F.; Liu, Y.; Luo, Y. Sedimentary characteristics of the Cambrian Canglangpu Formation in the central Sichuan Basin. *Lithol. Reserv.* **2022**, *34*, 19–31.
27. Liu, M.J.; Ji, Y.C.; Tang, Q.S.; Tang, D.H.; Liang, F.; Che, G.Q.; Wang, L.E.; Li, M.; Tan, X.C.; Zeng, W.; et al. Control of diagenetic system on tight sandstone reservoir quality: A case study of the second member of the Xujiahe Formation in the Zhongtaishan area, Sichuan Basin. *Acta Sedimentol. Sin.* **2021**, *39*, 826–840.
28. Ran, Q.; Lei, C.; Chen, K.; Zhang, B.J.; Liang, H.; Han, S.; Zeng, M.; Liu, X.B.; Pi, X.J.; Guan, S.W. Structural deformation characteristics, evolution and petroleum geological significance of the northwestern Sichuan Basin. *Chin. J. Geol.* **2023**, *58*, 18–35.
29. Guo, T.L.; Xiong, L.; Lei, W.; Zhao, Y.; Pang, H.Q. Exploration and development progress, challenges and reflections of deep shale gas in the Weirong and Yongchuan areas, southern Sichuan Basin. *Nat. Gas Ind.* **2022**, *42*, 45–59.
30. Zheng, M.J.; Guo, X.W.; Wu, Y.; Zhao, W.T.; Deng, Q.; Xie, W.Y.; Ou, Z.P. Practice of geological-engineering integration high-yield well cultivation and exploration breakthrough of ultra-deep shale gas in the Cambrian Qiongzhusi Formation of the Deyang-Anyue Rift Trough, Sichuan Basin. *China Pet. Explor.* **2024**, *29*, 57–67.
31. Yong, R.; Wu, J.F.; Wu, W.; Yang, Y.R.; Xu, L.; Luo, C.; Liu, J.; He, Y.F.; Zhong, K.S.; Li, Y.Y.; et al. Exploration discovery and significance of shale gas in the Cambrian Qiongzhusi Formation of the Sichuan Basin. *Acta Pet. Sin.* **2024**, *45*, 1309–1323.
32. Xiong, L.; Deng, H.C.; Wu, D.; Wei, L.M.; Wang, T.; Zhou, H.; Cao, K.X.; Xie, X.H.; Ma, R.L.; Zhong, Y.T. Fine-grained sedimentary characteristics and influencing factors of the Lower Cambrian Qiongzhusi Formation in the Sichuan Basin and its surrounding areas. *Pet. Geol. Exp.* **2023**, *45*, 857–871.
33. Li, S.J.; Sun, D.S.; Zheng, M.L.; Meng, X.W. Salt—Related structures and their hydrocarbon—Controlling effects in the Cambrian of the Sichuan Basin. *Oil Gas Geol.* **2014**, *35*, 622–631, 638.
34. Liu, M.C.; Yang, W.; Li, Q.R.; Ma, Y.L.; Zhu, Q.Y.; Xie, Z.Y.; Jin, H.; Shi, Z.S.; Shen, Y.J. Study on stratigraphic division and correlation of the Cambrian in the southern Sichuan Basin. *Nat. Gas Geosci.* **2008**, *19*, 100–106.
35. Chen, M.S.; Zhang, B.J.; Li, Z.W.; Liu, S.G.; Li, Y.; Song, J.M.; Wang, H.; Jiang, H.; Wang, L.K.; Xu, S.L.; et al. Lithological–carbon isotope stratigraphic division and significance of the Ediacaran Dengying Formation in the Sichuan Basin and its surrounding areas. *J. Palaeogeogr.* **2023**, *25*, 1347–1363.
36. Gu, M.F.; Liu, R.; Zhang, H.; He, Y.; Li, K.Y.; Hao, Y.; Jiang, H.; Li, W.Z. Characteristics and geological responses of the Caledonian tectonic movement in the Sichuan Basin. *Nat. Gas Ind.* **2023**, *43*, 32–43.
37. Zhou, C.Y.; He, Y.; Li, Z.Z.; Zhou, G.; Yang, D.L.; Sun, Y.T.; Zhang, Y.; Wen, H.G.; Liu, S.B. Micropore characteristics and genesis of carbonate rocks in the first member of the Lower Cambrian Canglangpu Formation in the north-central Sichuan Basin. *Pet. Geol. Exp.* **2025**, *47*, 311–322.
38. Wang, W.Z.; Fan, Y.; Lai, Q.; Zhou, G.; Nie, J.; Deng, S.S. New understanding of dolomite distribution and its petroleum geological significance in the Lower Cambrian Canglangpu Formation of the Sichuan Basin. *Nat. Gas Explor. Dev.* **2018**, *41*, 1–7.
39. Li, Y.D.; Chen, Y.L.; Yan, W.; Dai, R.X.; Xi, C.; He, Y. Sedimentary evolution characteristics of the Cambrian Canglangpu Formation in the Sichuan Basin. *Nat. Gas Geosci.* **2021**, *32*, 1334–1346.
40. Peng, J.; Chu, J.T.; Chen, Y.L.; Wen, J.; Li, Y.D.; Deng, S.S. Sedimentary characteristics of the Lower Cambrian Canglangpu Formation in the Gaoshiti–Moxi area of the Sichuan Basin. *Lithol. Reserv.* **2020**, *32*, 12–22.
41. Le, H.; Zhao, L.Z.; Yang, Y.; Xie, J.R.; Wen, L.; Luo, B.; He, Y.; Chen, Y.L.; Wang, W.Z. Major exploration discoveries of oil and gas in the Cambrian Canglangpu Formation of the Sichuan Basin and their implications. *Nat. Gas Ind.* **2020**, *40*, 11–19.
42. Li, S.S.; Jiang, P.F.; Liu, L.; Lei, C.; Zeng, Y.X.; Chen, S.Z.; Zhou, G. Seismic response characteristics and distribution law of carbonate grain banks in the Cambrian Canglangpu Formation of the Gaomo area, Sichuan Basin. *Lithol. Reserv.* **2022**, *34*, 22–31.
43. Yan, W.; Luo, B.; Zhou, G.; Chen, Y.L.; Zhong, Y.; Li, K.Y.; Zhou, H.F.; Zhao, L.K.; He, Y. Natural gas geological characteristics and exploration directions of the lower member of the Cambrian Canglangpu Formation in the Central Sichuan Paleouplift. *Pet. Explor. Dev.* **2021**, *48*, 290–302. [CrossRef]
44. Yan, W.; Zhong, Y.; Zhou, G.; Chen, Y.L.; He, Y.; Wang, W.Z.; Li, Y.D.; Chen, X.; Xi, C. Lithofacies palaeogeographic characteristics of the Lower Cambrian Canglangpu Formation in the Sichuan Basin and their controlling effects on reservoir development. *Nat. Gas Explor. Dev.* **2020**, *43*, 22–32.
45. Tong, Z.B.; Hu, Z.G.; Li, S.L.; Huang, Y.F.; Zuo, Y.A.; Zhu, Y.X.; Pang, Y.L.; Dong, Q.M.; Xu, C.Y. Silicate and carbonate mixed shelf formation and its controlling factors, a case study from the Cambrian Canglangpu formation in Sichuan basin, China. *Open Geosci.* **2023**, *15*, 20220480. [CrossRef]
46. Zou, B.; Qu, H.Z.; Zhao, R.R.; Zhang, L.J.; Zhang, Y.; Ma, Z.K.; Zhang, X.Y.; Huang, Q.Y.; Mo, Q.W.; An, H.Y.; et al. Diagenesis of the first member of Canglangpu Formation of the Cambrian series 2 in northern part of the central Sichuan Basin and its influence on porosity. *Front. Earth Sci.* **2023**, *10*, 1059838. [CrossRef]

47. Li, J.; Hu, Z.G.; Jiang, M.Y.; Liu, H.; Yang, M.D. Simultaneous determination of 13 elements including Ca, Mg, Sr and Ba in carbonate rocks by inductively coupled plasma atomic emission spectrometry (ICP—AES) with microwave digestion. *Chin. J. Inorg. Anal. Chem.* **2023**, *13*, 94–99.
48. Shen, C.C.; Wu, C.C.; Liu, Y.; Yu, J.M.; Chang, C.C.; Lam, D.D.; Chou, C.J.; Li, L.; Wei, K.Y. Measurements of natural carbonate rare earth elements in femtogram quantities by inductive coupled plasma sector field mass spectrometry. *Anal. Chem.* **2011**, *83*, 6842–6848. [CrossRef] [PubMed]
49. Bellefroid, E.J.; Planavsky, N.J.; Miller, N.R.; Brand, U.; Wang, C. Case studies on the utility of sequential carbonate leaching for radiogenic strontium isotope analysis. *Chem. Geol.* **2018**, *497*, 88–99. [CrossRef]
50. Lu, F.; Tan, X.; Wang, L.; Xiao, D.; Dong, S.; Su, C.; Pan, Z. Characteristics and Controlling Factors of Dolomite Reservoirs within Shoalcontrolled Karst in the Middle Permian Qixia Formation, Central Sichuan. *Basin Acta Sedimentol. Sin.* **2021**, *39*, 456–469.
51. Wang, H.; Qi, M.; Sun, F. The study of complex carbonate reservoir feature and its impact on oilfield development in Asmari Formation in A Oilfield, Iraq. *Adv. Geosci.* **2019**, *9*, 383–389. [CrossRef]
52. Li, B.; Goldberg, K. Diagenesis and reservoir quality of Cambrian carbonates in the Tarim Basin, northwestern China. *J. Asian Earth Sci.* **2022**, *223*, 104972. [CrossRef]
53. Yasuhara, H.; Elsworth, D.; Polak, A. Evolution of permeability in a natural fracture: Significant role of pressure solution. *J. Geophys. Res. Solid Earth* **2004**, *109*. [CrossRef]
54. Lang, P.S.; Paluszny, A.; Zimmerman, R.W. Hydraulic sealing due to pressure solution contact zone growth in siliciclastic rock fractures. *J. Geophys. Res. Solid Earth* **2015**, *120*, 4080–4101. [CrossRef]
55. Li, H.; Yu, F.S.; Wang, M.; Wang, Y.F.; Liu, Y.L. Quantitative prediction of structural fractures in the Paleocene lower Wenchang formation reservoir of the Lufeng Depression. *Adv. Geo-Energy Res.* **2022**, *6*, 375–387. [CrossRef]
56. Dempsey, D.; Kelkar, S.; Davatzes, N.; Hickman, S.; Moos, D. Numerical modeling of injection, stress and permeability enhancement during shear stimulation at the Desert Peak Enhanced Geothermal System. *Int. J. Rock Mech. Min. Sci.* **2015**, *78*, 190–206. [CrossRef]
57. Feng, K.; Yu, B.; Zhang, D. Experimental study on deformation and permeability enhancement of oil sand reservoir by hydraulic fracturing technique under true triaxial stress. *Energy Sci. Eng.* **2022**, *10*, 853–865. [CrossRef]
58. Sun, J.M.; Chi, P.; Cheng, Z.G.; Yang, L.; Yan, W.C.; Cui, L.K. A novel saturation calculation model of fractured-vuggy carbonate reservoir via multiscale pore networks: A case study from Sichuan Basin, China. *J. Geophys. Eng.* **2021**, *18*, 85–97. [CrossRef]
59. Gong, L.; Su, X.C.; Gao, S.; Fu, X.F.; Jabbari, H.; Wang, X.X.; Liu, B.; Yue, W.T.; Wang, Z.S.; Gao, A. Characteristics and formation mechanism of natural fractures in the tight gas sandstones of Jiulongshan gas field, China. *J. Pet. Sci. Eng.* **2019**, *175*, 1112–1121. [CrossRef]
60. Ren, G.X.; Qin, Q.R.; Qin, Z.J.; Guo, Y.B.; Ye, Z.Y. Effects of diagenesis on quality of deep dolomite reservoirs: A case study of the Upper Cambrian Xixiangchi Formation in the eastern Sichuan Basin, China. *Front. Earth Sci.* **2022**, *10*, 984463. [CrossRef]
61. Manniello, C.; Agosta, F.; Todaro, S.; Cavalcante, F.; Prosser, G. Fracture stratigraphy of Mesozoic platform carbonates, Agri Valley, southern Italy. *Geol. Mag.* **2022**, *159*, 1874–1896. [CrossRef]
62. Li, H.; Tang, H.M.; Qin, Q.R.; Wang, Q.; Zhong, C. Effectiveness evaluation of natural fractures in Xujiahe Formation of Yuanba area, Sichuan basin, China. *Arab. J. Geosci.* **2019**, *12*, 194. [CrossRef]
63. Huang, H.X.; Wen, H.G.; Wen, L.; Zhang, B.J.; Zhou, G.; He, Y.; Wen, L.B.; Zhao, Y.; Jiang, H.C. Multistage dolomitization of deeply buried dolomite in the Lower Cambrian Canglangpu Formation, central and northern Sichuan Basin. *Mar. Pet. Geol.* **2023**, *152*, 106261. [CrossRef]
64. Tan, Q.; Shi, Z.J.; Tian, Y.M.; Wang, Y.; Li, W.J. Petrological and geochemical constraints on the origin of dolomites: A case study from the early Cambrian Qingxudong Formation, Sichuan Basin, South China. *Carbonates Evaporites* **2019**, *34*, 1639–1656. [CrossRef]
65. Fu, S.Y.; Zhang, C.G.; Chen, H.D.; Qing, H.R. Geochemistry characteristics and dolomitization mechanism of the Upper Cambrian dolomite, eastern Ordos Basin, China. *Geol. J.* **2020**, *55*, 3070–3082. [CrossRef]
66. Veizer, J.; Ala, D.; Azmy, K.; Bruckschen, P.; Buhl, D.; Bruhn, F.; Carden, G.A.F.; Diener, A.; Ebneth, S.; Godderis, Y. 87Sr/86Sr, δ13C and δ18O evolution of Phanerozoic seawater. *Chem. Geol.* **1999**, *161*, 59–88. [CrossRef]
67. Li, L.P.; Wen, H.G.; Zhou, G.; Luo, B.; Liang, J.T.; Liu, S.B.; Li, K.Y.; Guo, Y.B.; Hu, W.W. Petrographic, rare earth elemental and isotopic constraints on the dolomite origin: A case study from the middle-upper Cambrian Xixiangchi Formation in Eastern Sichuan Basin, Southwest China. *Minerals* **2022**, *12*, 1224. [CrossRef]
68. Hu, H.; Xu, S.L.; Chen, A.Q.; Wen, L.; Zhang, B.J.; Zhang, X.H.; Li, F.X.; Liu, M.Q.; Yong, W. The Origin of the Upper Cambrian Basin-Scale Massive Dolostones of the Xixiangchi Formation, Sichuan Basin, China. *Minerals* **2023**, *13*, 932. [CrossRef]
69. Kochnev, B.B.; Pokrovsky, B.G.; Kuznetsov, A.B.; Marusin, V.V. C and Sr isotope chemostratigraphy of Vendian–Lower Cambrian carbonate sequences in the central Siberian Platform. *Russ. Geol. Geophys.* **2018**, *59*, 585–605. [CrossRef]

70. Ning, M.; Wang, Y.; McKenzie, J.A.; Vasconcelos, C.; Li, C.Q.; Shen, A.J.; Liang, F.; Shen, B. Dolomite formation during penecontemporaneous subaerial diagenesis: Evidence from modern dolomite crusts forming in lagoon Brejo do Espinho, Brazil. *J. Geol. Soc.* **2024**, *181*, jgs2023–jgs2159. [CrossRef]
71. Wostbrock, J.A.G.; Brand, U.; Coplen, T.B.; Swart, P.K.; Carlson, S.J.; Brearley, A.J.; Sharp, Z.D. Calibration of carbonate-water triple oxygen isotope fractionation: Seeing through diagenesis in ancient carbonates. *Geochim. Cosmochim. Acta* **2020**, *288*, 369–388. [CrossRef]
72. Gregg, J.M.; Shelton, K.L. Dolomitization and dolomite neomorphism in the back reef facies of the Bonneterre and Davis formations (Cambrian), southeastern Missouri. *J. Sediment. Res.* **1990**, *60*, 549–562. [CrossRef]
73. Machel, H.G. Concepts and models of dolomitization: A critical reappraisal. *Geol. Soc.* **2004**, *235*, 7–63. [CrossRef]
74. McArthur, J.M.; Kennedy, W.J.; Gale, A.S.; Thirlwall, M.F.; Chen, M. Strontium isotope stratigraphy in the Late Cretaceous: IntercontinentaI correlation of the Campanian/Maastrichtian boundary. *Terra Nova* **1992**, *4*, 385–393. [CrossRef]
75. Zhang, X.J.; Zhou, G.; Zhang, P.Y.; He, Y.; Wei, Z.F.; Wang, G.; Zhang, T.; He, W.; Ma, H.; Zhu, C.X. Strontium isotope and element constraints on the paleoenvironment of the latest Ediacaran in the Sichuan Basin, southeastern Tibetan Plateau. *Front. Earth Sci.* **2022**, *10*, 865709. [CrossRef]
76. Zheng, H.F.; Ma, Y.S.; Chi, G.X.; Qing, H.R.; Liu, B.; Zhang, X.F.; Shen, Y.C.; Liu, J.Q.; Wang, Y.C. Stratigraphic and structural control on hydrothermal dolomitization in the Middle Permian carbonates, southwestern Sichuan Basin (China). *Minerals* **2019**, *9*, 32. [CrossRef]
77. Malone, M.J.; Baker, P.A.; Burns, S.J. Recrystallization of dolomite: Evidence from the Monterey Formation (Miocene), California. *Sedimentology* **1994**, *41*, 1223–1239. [CrossRef]
78. Xiong, Y.; Tan, X.C.; Dong, G.D.; Wang, L.C.; Ji, H.K.; Liu, Y.; Wen, C.X. Diagenetic differentiation in the Ordovician Majiagou Formation, Ordos Basin, China: Facies, geochemical and reservoir heterogeneity constraints. *J. Pet. Sci. Eng.* **2020**, *191*, 107179. [CrossRef]
79. Khan, S.; Shah, M.M. Multiphase dolomitization in the Jutana Formation (Cambrian), Salt Range (Pakistan): Evidences from field observations, microscopic studies and isotopic analysis. *Geol. Acta* **2019**, *17*, 0002. [CrossRef]
80. Chen, Z.P.; Yang, Y.F.; Dong, C.Y.; Li, N.X.; Wang, P.T.; Zhang, S.H.; Dang, W.; Liao, Y. Genesis of Cambrian Dolomites in the Bachu Area, Tarim Basin, NW China: Constraints from petrology, geochemistry, and fluid inclusions. *Minerals* **2022**, *12*, 1157. [CrossRef]
81. Gray, E.; Hartley, A.; Howell, J. The influence of stratigraphy and facies distribution on reservoir quality and production performance in the Triassic Skagerrak Formation of the UK and Norwegian Central North Sea. *Geol. Soc.* **2022**, *494*, 379–409. [CrossRef]
82. Zhou, J.G.; Xu, C.C.; Yao, G.S.; Yang, G.; Zhang, J.Y.; Hao, Y.; Wang, F.; Pan, L.Y.; Gu, M.F.; Li, J.Y. Genesis and evolution of lower Cambrian Longwangmiao formation reservoirs, Sichuan Basin, SW China. *Pet. Explor. Dev.* **2015**, *42*, 175–184. [CrossRef]
83. Lei, C.; Xu, S.H.; Zhang, W.; Li, Y.H.; Li, M.; Wu, C.; Wu, S.H.; Shang, W.L.; Luo, K.T.; Li, X.G. Prediction of grain shoal reservoirs via seismic forward modeling and waveform classification: Application to the northern slope of the central Sichuan Uplift, Sichuan Basin, SW China. *Interpretation* **2024**, *12*, T555–T571. [CrossRef]
84. Andersson, A.J. A fundamental paradigm for coral reef carbonate sediment dissolution. *Front. Mar. Sci.* **2015**, *2*, 52. [CrossRef]
85. Neveux, L.; Grgic, D.; Carpentier, C.; Pironon, J.; Girard, J.P. Influence of hydrocarbon injection on the compaction by pressure-solution of a carbonate rock: An experimental study under triaxial stresses. *Mar. Pet. Geol.* **2014**, *55*, 282–294. [CrossRef]
86. Wilkinson, M.; Haszeldine, R.S. Oil charge preserves exceptional porosity in deeply buried, overpressured, sandstones: Central North Sea, UK. *J. Geol. Soc.* **2011**, *168*, 1285–1295. [CrossRef]
87. Song, Y.F.; Chen, Y.; Lin, T.; Wang, M.; Tian, H. Direct evidence for abnormal overpressure generated by crude oil cracking in the Sinian Dengying Formation, Central Sichuan Basin, southwestern China. *AAPG Bull.* **2025**, *109*, 845–861. [CrossRef]
88. Fan, Q.Q.; Liu, D.D.; Du, W.; Li, Y.M.; Liang, F.; Zhao, F.P.; Feng, X.; Chen, Y.; Zhang, Z.Y.; Zhang, Y.X. In situ U-Pb dating of carbonate veins in Cambrian shales constrains fluid flow and hydrocarbon evolution at the southeastern margin of the Upper Yangtze platform, southwestern China. *Geol. Soc. Am. Bull.* **2024**, *136*, 2875–2890. [CrossRef]
89. Gao, F.; Pei, X.Z.; Li, R.B.; Li, Z.C.; Pei, L.; Chen, Y.X.; Wang, M.; Zhao, S.W.; Liu, C.J.; Li, X.B. Further constraints on a Neoproterozoic active continental margin from sandstones of the Hengdan Group in the Bikou Terrane, northwestern margin of the Yangtze Block, South China. *J. Asian Earth Sci.* **2020**, *203*, 104514. [CrossRef]
90. Li, W.Z.; Zhang, J.Y.; Zhu, X.J.; Wang, Y.X.; Tian, X.W.; Fu, X.D.; Jiang, H.; Zhong, Y.; Liu, S.G.; Li, R. Late Ediacaran to Early Cambrian stratigraphic correlation and its geological implications in the northwestern Sichuan Basin: Insights from phosphorus, isotopes, and small shelly fossils. *Front. Earth Sci.* **2024**, *12*, 1440117. [CrossRef]

91. Jiang, H.C.; Liang, J.T.; Azmy, K.; Cao, J.X.; Wen, L.; Zhou, G.; He, Y.; Liu, S.B.; Huo, F.; Wen, H.G. Controls of sedimentary facies and sealevel fluctuation on dolomitization: The Lower Cambrian Longwangmiao Formation in Sichuan Basin, China. *Mar. Pet. Geol.* **2023**, *157*, 106465. [CrossRef]
92. Bian, L.B.; Schovsbo, N.H.; Chappaz, A.; Rudra, A.; Xu, J.; Luo, Q.Y.; Sanei, H. Paleoenvironmental Reconstruction and Organic Matter Accumulation of the Lower Cambrian Qiongzhusi Formation in the Sichuan Basin, South China. *ACS Earth Space Chem.* **2022**, *6*, 2519–2529. [CrossRef]

Disclaimer/Publisher's Note: The statements, opinions and data contained in all publications are solely those of the individual author(s) and contributor(s) and not of MDPI and/or the editor(s). MDPI and/or the editor(s) disclaim responsibility for any injury to people or property resulting from any ideas, methods, instructions or products referred to in the content.